Preprints, 4th IFAC Conference on
Advances in Proportional-Integral-Derivative Control
Almería, Spain | June 12-14, 2024

Automating RTGC with PID Control: Utilizing Camera-Based Image Processing and Object Detection

Steven Bandong*, Yul Y. Nazaruddin, Augie Widyotriatmo**, Muhammad R. Miransyahputra**, Yan Setiaji****

** Engineering Physics Doctoral Program, Faculty of Industrial Technology, Institut Teknologi Bandung, Bandung, Indonesia (e-mail: bandong.steven@gmail.com).*

***Instrumentation, Control and Automation Research Group, Faculty of Industrial Technology, Institut Teknologi Bandung, Bandung, Indonesia (e-mail: yul@itb.ac.id, augie@itb.ac.id, raihanmiransyah@gmail.com, yan.setiaji@gmail.com)*

Abstract: The high traffic in the container yard requires effective management, and one method to address this is through automation. The Rubber Tyred Gantry Crane (RTGC) plays a crucial role in container yards. Automating the RTGC involves determining the container's location and sway angle to provide feedback for the control system. The advancements in computer vision technology offer a unique solution to tackle these challenges. This paper proposes image processing as a means to sense the sway angle and MobileNet SSD to detect the container's location. The proposed method yields accurate measurement results and is integrated with optimized PID-PD for position and sway angle control in RTGC. The effectiveness of the proposed method is demonstrated through successful performance in both simulation and experiments conducted on a laboratory-scale RTGC prototype.

Keywords: port automation, RTGC control system, computer vision, optimization, camera based sensor

1. INTRODUCTION

The volume of container shipments in international goods transactions has witnessed significant growth in recent decades (Carrese et al., 2022; Cho & Yang, 2011). This is exemplified by the continuous 24/7 operations at Tanjung Periok Port in Jakarta, underscoring the immense traffic of containers. Within the seaport, the container yard shoulders a substantial burden due to these factors (Ardi et al., 2017). Accidents, such as operator errors in handling Rubber Tyred Gantry Crane (RTGC) operations, can result in substantial losses of money, time, equipment, and even pose risks to life (Xie et al., 2021). In response, researchers have sought to mitigate these risks by introducing automation into RTGC operations within the container yard.

Control systems utilizing open-loop approaches, such as input shaping (Ho Duc et al., 2014; Singhose et al., 2000) and time-optimal control (Manson, 1982), have been explored to relocate containers to desired locations. Alternatively, closed-loop methods, including PID controllers, fuzzy control (Solihin et al., 2010), model predictive control (Singh & Agrawal, 2018), etc., have been investigated with a primary goal of moving containers to desired positions while minimizing sway angles during the process, where closed-loop methods exhibit commendable performance. However, challenges may arise in implementing closed-loop methods, particularly in measuring sway angles. Some researchers have utilized observers (Ogawa et al., 2021) as a potential solution, while this paper proposes an approach using computer vision and image processing.

Computer vision has gained popularity in various fields, including robotics (Dairath et al., 2023), medical (Esteva et al., 2021), and manufacturing (Grierson et al., 2021). It offers the capability to monitor, analyze, or obtain information from 2D image data. In this paper, these benefits are harnessed to automate RTGC operations. Leveraging recently developed fast object detection methods, especially the MobileNet SSD (Li et al., 2018), facilitates real-time control systems with high accuracy object detection while maintaining a high frames-per-second (fps) rate. This technology is applied to detect the container's location and sense its sway angle, enabling the implementation of a closed-loop controller with a camera-based sensor.

The paper employs two controllers to manage dynamics during the container transfer. PID is utilized for container position control, while PD is employed for sway angle control. Furthermore, three optimization methods, namely Particle Swarm Optimization (PSO), Stochastic Fractal Search (SFS), and Flower Pollination Algorithm (FPA), are employed to enhance performance. The designed control system is then integrated with the computer vision system. This approach is tested through simulation and in a laboratory-scale RTGC system, demonstrating promising control performance and providing valuable insights for researchers in the related field.

2. RTGC DYNAMICS

The RTGC system, as depicted in Fig. 1, consists of two main components to be controlled: the trolley position (x) with mass m_2 and the sway angle (θ) with payload mass m_2.The hoisting cable length is denoted as l, and the control force is F. The

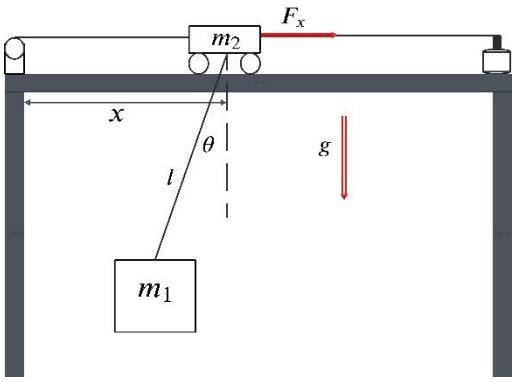

Figure 1. RTGC system representation

dynamic model is derived using the Lagrange equation, leading to the following dynamic equations

$$(m_1 + m_2)\ddot{x} + m_1 l\ddot{\theta}\cos\theta - m_1 l\dot{\theta}^2 \sin\theta + D\dot{x} = F \quad (1)$$

$$m_1 l^2\ddot{\theta} + m_1 l\ddot{x}\cos\theta + m_1\dot{x}l\dot{\theta}\sin\theta + m_1 gl\sin\theta = 0 \quad (2)$$

The dynamic model is then connected to the DC motor model (Solihin et al., 2010) as follows

$$V = \left(\frac{R.r_p}{K_t.r}\right)F + \frac{K_e.r}{r_p}\dot{x} \quad (3)$$

where V, R, r_p, r, K_t, K_e are DC motor input voltage, resistance, pulley radius, the ratio of wheel radius and pulley, torque constant, and electric constant, respectively. By substituting (1) into (3), the controlled RTGC system through DC motor voltage is obtained

$$V = \left(\frac{R.r_p}{K_t.r}\right)(m_1 + m_2)\ddot{x} + \left(\frac{D.R.r_p}{K_t.R} + \frac{K_e.r}{r_p}\right)\dot{x} + \left(\frac{m_1 l.R.r_p}{K_t.r}\right)\left(\ddot{\theta}\cos\theta - \dot{\theta}^2\sin\theta\right) \quad (4)$$

$$l^2\ddot{\theta} + l\ddot{x}\cos\theta + gl\sin\theta = 0 \quad (5)$$

The nonlinear system in (4) and (5) are then linearized under the assumption of a small sway angle ($\theta \approx 0$) where $\sin\theta \approx \theta$, $\cos\theta \approx 1$, and $\dot{\theta}^2 \approx 0$. The results are presented in (6) and (7)

$$V = \left(\frac{R.r_p}{K_t.r}\right)(m_1 + m_2)\ddot{x} + \left(\frac{D.R.r_p}{K_t.R} + \frac{K_e.r}{r_p}\right)\dot{x} + \left(\frac{m_1 l.R.r_p}{K_t.r}\right)\ddot{\theta} \quad (6)$$

$$l^2\ddot{\theta} + l\ddot{x} + gl\theta = 0 \quad (7)$$

The dynamics equation on (6) and (7) are represented on a state space equation as shown below

$$\begin{bmatrix}\dot{x}\\ \ddot{x}\\ \dot{\theta}\\ \ddot{\theta}\end{bmatrix} = \begin{bmatrix}0 & 1 & 0 & 0\\ 0 & \frac{-b}{a-\frac{c}{l}} & \frac{c\,g}{l\left(a-\frac{c}{l}\right)} & 0\\ 0 & 0 & 0 & 1\\ 0 & \frac{b}{a\left(l-\frac{c}{a}\right)} & \frac{-g}{l-\frac{c}{a}} & 0\end{bmatrix}\begin{bmatrix}x\\ \dot{x}\\ \theta\\ \dot{\theta}\end{bmatrix} + \begin{bmatrix}0\\ \frac{1}{a-\frac{c}{l}}\\ 0\\ \frac{-1}{a\left(l-\frac{c}{a}\right)}\end{bmatrix}V \quad (8)$$

$$y = \begin{bmatrix}1 & 0 & 0 & 0\\ 0 & 0 & 1 & 0\end{bmatrix}\begin{bmatrix}x\\ \dot{x}\\ \theta\\ \dot{\theta}\end{bmatrix} + \begin{bmatrix}0\\ 0\end{bmatrix}u \quad (10)$$

where

$$a = \left(\frac{R.r_p}{K_t.r}\right)(m_1 + m_2)\,;\ \mathrm{b} = \left(\frac{D.R.r_p}{K_t r} + \frac{K_e.r}{r_p}\right);\ c = \left(\frac{m_1 l.R.r_p}{K_t.r}\right)$$

3. CONTROL SYSTEM DESIGN AND OPTIMIZATION

Table 1. Optimization Algorithm Parameters

Parameter	PSO	SFS	FPA
Iteration	500		
Population (M)	20		
Particle (K)	5		
$w(max, \min)$	0.9 0.4		
c_1	2		
c_2	2		
$\mathcal{D}$		3	
GW Probability		0.5	
λ			1.5
switch p Probability			0.5

The PID-PD controller is proposed for use in the system. To obtain optimal controller parameters, Particle Swarm Optimization (PSO), Stochastic Fractal Search (SFS), and Flower Pollination Algorithm (FPA) are employed, each with specific search parameters outlined in Table 1. The loss function in (11) is formulated to be minimized by the optimization algorithm

$$J = \int_{t_0}^{t_r} t\left(x - x_{ref}\right)^2 dt + \int_{t_r}^{t_{end}} t(\theta)^2 dt + \int_{t_s}^{t_{end}} t\left(x - x_{ref}\right)^2 dt \quad (11)$$

with t_0 representing the initial time of simulating the system, and t_r(4s), t_s(6s) and t_{end} (8s) being the values for rise time, settling time and simulation ending time based on the reference trajectory. x and θ represent the outputs of the trolley position and the container swing angle from the model, while x_{ref} is the reference trajectory as depicted on Fig. 2.

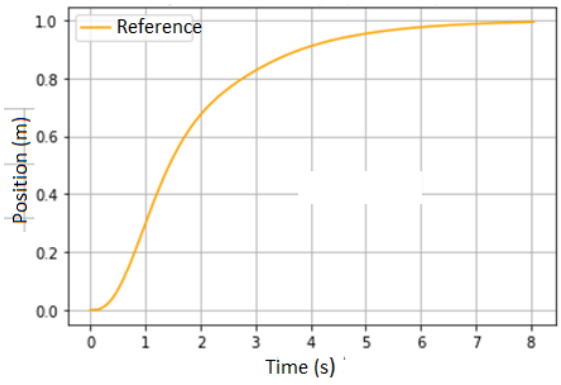

Figure 2. Reference trajectory (x_{ref})

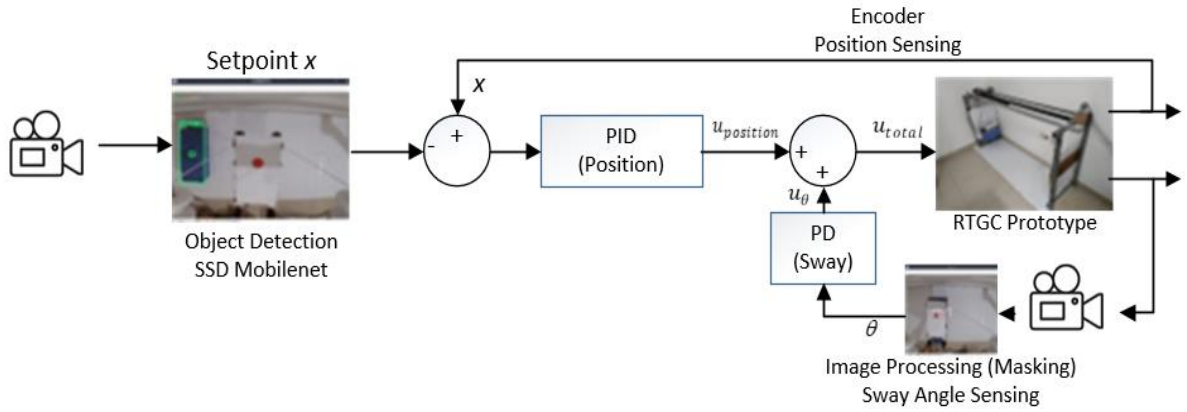

Figure 3. The designed control system

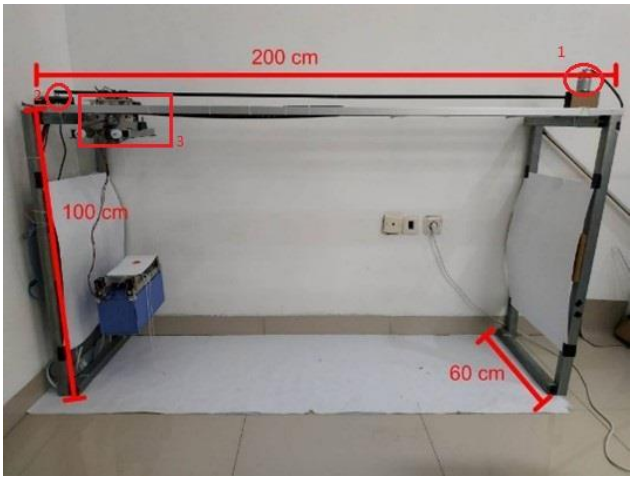

Figure 4. Gantry Crane Prototype

A PID controller is employed for position control, while PD is used for the sway angle controller. A total of 5 parameters of the controller K_P, K_I, K_D, K_{PS} and K_{DS}, require optimization. The optimal parameters obtained are utilized in the control system designed in the scheme depicted in Fig.3. The gantry crane prototype, where the experiment is being held, is shown in Fig.4. The actuator for control is a DC motor, shown as circle number 1 in Fig.4. The trolley's position is obtained through an encoder (circle number 2 in Fig.4), and the sway angle is determined using a computer vision method, which will be discussed in the next section. The camera for computer vision techniques is installed on the RTGC trolley, as depicted in box number 3 in Fig. 4. These two pieces of information serve as feedback in this control system, forming a closed-loop control.

4. SWAY ANGLE SENSING BASED ON COMPUTER VISON

The advancement in computer vision technology in recent years has sparked a growing interest in its application for automating various industries. In the field of control systems, there is a need for sensing technology to operate swiftly for real-time applications. Therefore, in this paper, the MobileNet SSD algorithm is employed to sense the sway angle of the RTGC through an object detection approach. A dataset of 1000 container images was collected and annotated to train the MobileNet SSD. The resulting bounding boxes are utilized to measure distances in pixel terms, which are then converted to meters using a scaling method. Additionally, a red circle is drawn around the spreader, and by employing color masking, the sway angle of the spreader is obtained, as illustrated in Fig. 5.

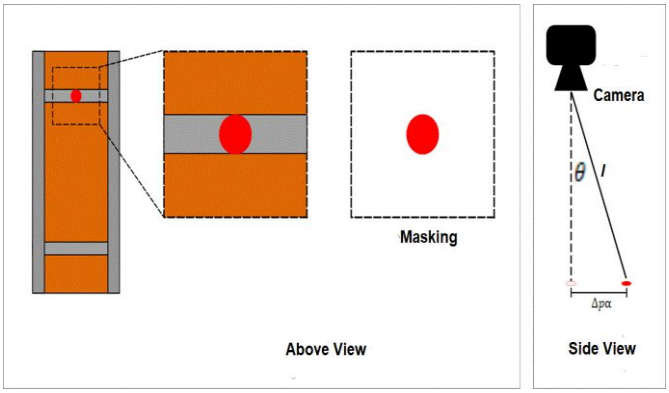

Figure 5. Design calculation of container swing angle.

The sway angle of the spreader with container then can be obtained using the following formulae

$$\sin\theta \approx \theta = \frac{\Delta p\alpha}{l} \tag{12}$$

where θ is the swing angle of the load in radians with asumption small angle $\sin\theta \approx \theta$. Δp is the pixel deviation (px), l is the length of the load rope (m), and α is the conversion factor (m/px).

Object detection is performed using SSD MobileNet to determine the container's position in terms of pixels, which is then converted to meters. This information becomes the setpoint for the control system, as illustrated in Fig. 3. Fig. 6 demonstrates the results of the container detection.

Figure 6. Container detection results

The object detection algorithm, the load swing angle measurement algorithm, and the camera are integrated with the gantry crane control system. Object detection by the camera is processed to obtain input position for the control system. Subsequently, the output trolley position from the encoder is fed back to the PID-position controller, resulting in the signal $u_{position}$ Similarly, the output load swing angle is fed back through the PD-swing controller, generating the signal u_θ. The u_θ signal then be summed with the $u_{position}$, forming a single u_{total} signal as the RTGC control input. This input signal will affect the DC motor voltage that drives the trolley, as shown in Fig. 3. The proposed control system scheme will be simulated and then tested on a laboratory-scale RTGC prototype.

5. RESULTS AND ANALYSIS

The optimization progress and the resulting optimized PID-PD parameters for the RTGC control system are presented in Fig. 7 and Table 2. These three optimization methods have minimized the loss function, with FPA providing the smallest loss function value, achieved in 9 minutes of processing time on a CPU with Intel Core i7 10750H.

These optimized parameters are then tested on simulation and also in the real time experiment on a laboratory scale prototype of RTGC. Based on Fig.8–10, it can be observed from the plotted graphs that the displacement position system's response in the prototype already exhibits a trajectory similar to the simulation. However, in the RTGC sway angle response, a noticeable difference can be seen. In the simulation, there are only two angle deviations before reaching a steady position, while in the prototype movement, there is still a small oscillation after passing the first two deviations. Oscillations occur for approximately ± 5 seconds before the load swing returns to its normal position. A similar phenomenon occurs for all three different controller gains. Therefore, an analysis related to the dynamic characteristics of the system is conducted to further examine the system's response in detail, as presented in Table 3.

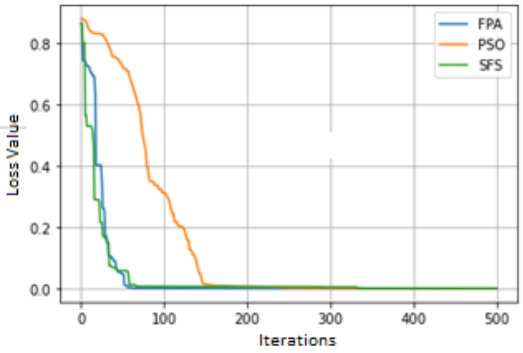

Figure 7. Convergence of loss value during optimization

Table 2. Optimization Results

Gain	PSO	SFS	FPA
K_P	5.74058	5.65467	5.80958
K_I	0.01120	0.02142	0.00180
K_D	0.31320	0.21195	-0.16632
K_{PS}	16.4573	13.9750	11.6932
K_{DS}	8.47020	8.07139	5.55599
Loss value	0.00087	0.00147	0.00043
Runtime	7 m 47 s	23 m 29 s	9 m 2 s

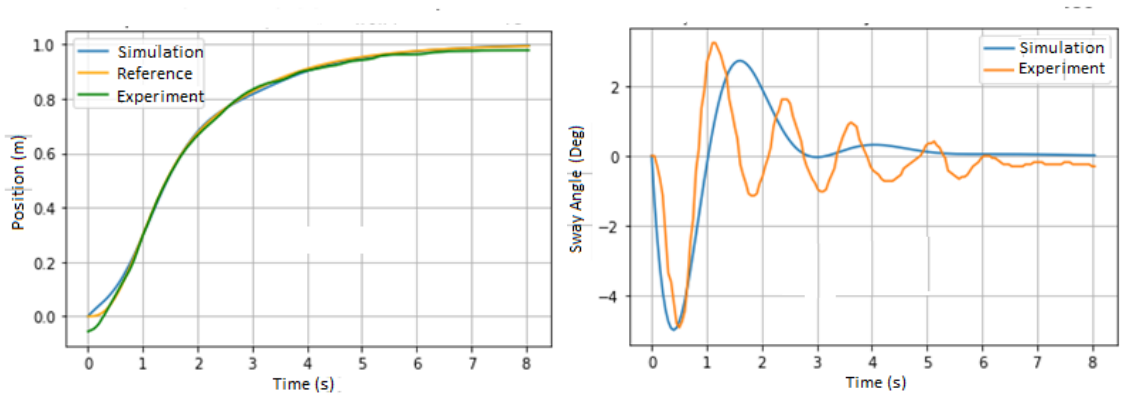

Figure 8. PSO-PID-PD control results

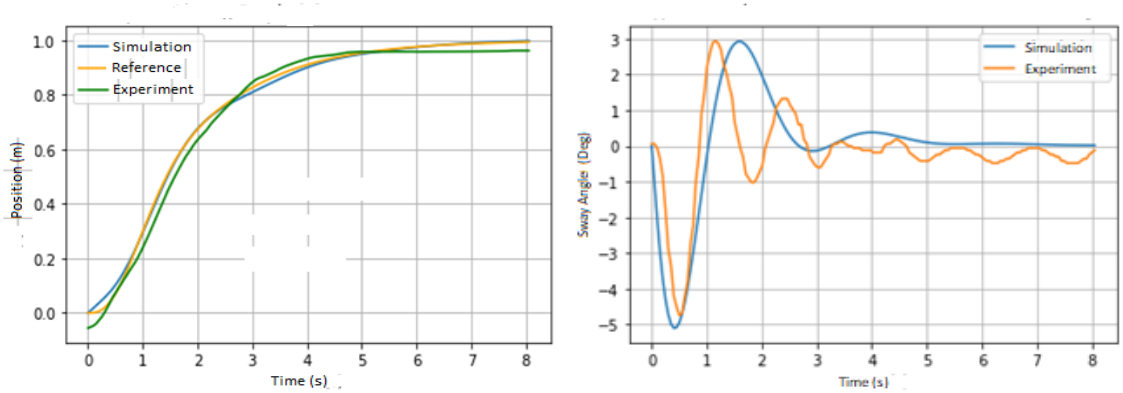

Figure 9. SFS-PID-PD control results

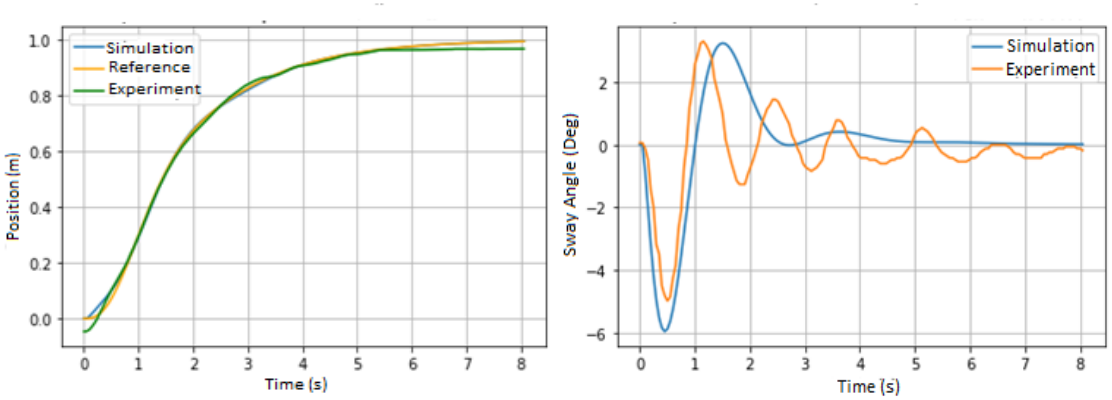

Figure 10. FPA-PID-PD control results

Table 3. Position Control Results

Parameter	PSO		SFS		FPA	
	Sim.	**Exp.**	**Sim.**	**Exp.**	**Sim.**	**Exp.**
Steady State Error(cm)	0.46	2.00	0.22	4.00	0.60	3.00
Overshoot (%)	0.0	0.0	0.0	0.0	0.0	0.0
Rise Time (s)	3.90	3.75	3.95	3.20	3.80	3.50
Settling Time (s)	6.00	5.30	6.10	4.25	5.85	4.95

Sim.: Simulation, **Exp.:** Experiment on prototype, Best on simulation, Best on experiment

Table 4. Sway Angle Control Results

Parameter	PSO		SFS		FPA	
	Sim.	**Exp.**	**Sim.**	**Exp.**	**Sim.**	**Exp.**
Maximum Positive Amplitude	2.732º	3.244º	2.928º	2.943º	3.247º	3.304º
Maximum Negative Amplitude	-4.998º	-4.926º	-5.103º	-4.745º	-5.963º	-4.986º
Steady State Error	0.0000º	±0.0010º	0.0000º	±0.0010º	0.0000º	±0.0049º

Sim.: Simulation, **Exp.:** Experiment on prototype, Best on simulation, Best on experiment

Table 3 provides the system performance in the simulation, allowing for a comparison with the results obtained from the prototype. For the steady-state error parameter, the best result in the simulation was obtained from the SFS assessment with an error of 0.22 cm, while for the actual prototype, the best result was obtained from the PSO assessment with an error of 2 cm. For the overshoot parameter, all system responses demonstrated good performance by not producing overshoot values. With regard to the rise time and settling time parameters, the SFS assessment yielded the best performance in the prototype with a rise time of 3.20 seconds and settling time of 4.25 seconds. In contrast, in the simulation, the best performance was provided by the FPA assessment with a rise time of 3.80 seconds and settling time of 5.85 seconds.

For the assessment of the container swing angle system's response, the measured parameters include the maximum positive deviation, maximum negative deviation, and steady-state error. The steady-state error mentioned here refers to the deviation condition when the acquisition process is halted. The acquisition process is conducted for a duration of 8 seconds, aiming for a steady-state system at the 6 second. Regarding the deviation parameters, in the simulation, the best performance is provided by the PSO assessment with deviations of 2.7° and -4.9°. On the other hand, in the prototype performance, the best result is achieved through the SFS assessment with deviations of 2.9° and -4.7°. Subsequently, for the steady-state error parameter, simulation results indicate all values are 0, whereas for the prototype response, the best result is obtained from the SFS assessment.

6. CONCLUSIONS

The paper proposes the integration of advancements in computer vision into the automation of Rubber Tyred Gantry Crane (RTGC). The system is designed with a sensor system based on image processing to infer the sway angle and MobileNet SSD to detect the container's position. Furthermore, an optimized PID-PD is employed to move the container to the desired position while minimizing sway during the process. The results demonstrate that the camera-based sensor system successfully senses the sway angle and detects the position of the container. Additionally, the control system provides good results both in simulation and in experiments conducted on the prototype of RTGC. Further investigation will be conducted based on a nonlinear control system integrated with LiDAR to sense the sway angle and position of the container.

ACKNOWLEDGMENT

This work was supported by Institut Teknologi Bandung Research Program 2024.

REFERENCES

Ardi, P. G., Ayu, A. G., & others. (2017). Safety management on loading process with rubber tyred gantry crane: case study at port of Tanjung Priok. *Russian Journal of Agricultural and Socio-Economic Sciences*, *66*(6), 150–164.

Carrese, S., Petrelli, M., & Renna, A. (2022). A new approach for the identification of strategic Italian ports for container traffic. *Transport Policy*, *120*. https://doi.org/10.1016/j.tranpol.2022.03.005

Cho, H. S., & Yang, K. W. (2011). Identifying country environments to increase container traffic volumes. *Asian Journal of Shipping and Logistics*, *27*(1). https://doi.org/10.1016/S2092-5212(11)80007-6

Dairath, M. H., Akram, M. W., Mehmood, M. A., Sarwar, H. U., Akram, M. Z., Omar, M. M., & Faheem, M. (2023). Computer vision-based prototype robotic picking cum grading system for fruits. *Smart Agricultural Technology*, *4*. https://doi.org/10.1016/j.atech.2023.100210

Esteva, A., Chou, K., Yeung, S., Naik, N., Madani, A., Mottaghi, A., Liu, Y., Topol, E., Dean, J., & Socher, R. (2021). Deep learning-enabled medical computer vision. In *npj Digital Medicine* (Vol. 4, Issue 1). https://doi.org/10.1038/s41746-020-00376-2

Grierson, D., Rennie, A. E. W., & Quayle, S. D. (2021). Machine Learning for Additive Manufacturing. *Encyclopedia*, *1*(3). https://doi.org/10.3390/encyclopedia1030048

Ho Duc, T., Nguyen, H., & Nguyen, Q. C. (2014). Input shaping Control of an Overhead Crane. *Vietnam Conference on Mechatronics*, *November 2014*.

Li, Y., Huang, H., Xie, Q., Yao, L., & Chen, Q. (2018). Research on a surface defect detection algorithm based on MobileNet-SSD. *Applied Sciences (Switzerland)*, *8*(9). https://doi.org/10.3390/app8091678

Manson, G. A. (1982). Time-optimal control of an overhead crane model. *Optimal Control Applications and Methods*, *3*(2), 115–120.

Ogawa, H., Yamada, T., & Nakamoto, M. (2021). Improved estimation of sway-angle for overhead crane based on phase difference of acoustic signals in frequency domain. *Proceedings of International Conference on Artificial Life and Robotics*, *2021*. https://doi.org/10.5954/icarob.2021.os10-6

Singh, A. P., & Agrawal, H. (2018). A fractional model predictive control design for 2-D gantry crane system. *Journal of Engineering Science and Technology*, *13*(7).

Singhose, W., Porter, L., Kenison, M., & Kriikku, E. (2000). Effects of hoisting on the input shaping control of gantry cranes. *Control Engineering Practice*, *8*(10), 1159–1165. https://doi.org/10.1016/S0967-0661(00)00054-X

Solihin, M. I., Wahyudi, & Legowo, A. (2010). Fuzzy-tuned PID anti-swing control of automatic gantry crane. *Journal of Vibration and Control*, *16*(1), 127–145.

Xie, T., Lu, X., Wang, G., & Lin, F. (2021). Research on Safety Risk, Prevention and Control in Port Dangerous Goods Container Yard. *Journal of Physics: Conference Series*, *1910*(1). https://doi.org/10.1088/1742-6596/1910/1/012029